Structure of igniting ethanol and n-heptane spray flames with and without swirl

C. Letty*, E. Mastorakos*, A.R. Masri, M. Juddoo** and W. O'Loughlin****
cl447@cam.ac.uk
* Engineering Department, University of Cambridge, Cambridge CB2 1PZ, UK
** School University of Sydney, NSW 2006, Australia

Abstract
This paper explores the ignition and subsequent evolution of spray flames in a bluff-body configuration with and without swirl. Ethanol and n-heptane are used to compare the effects of volatility. Ignition is performed by a laser spark. High speed imaging of OH*-chemiluminescence and OH-PLIF collected at 5 kHz are used to investigate the behaviour of the flames during the first stages of ignition and the stable flame structure following ignition. Swirl induces a wider and shorter flame, precession, and multiple reaction zones, while the non-swirling flames have a simpler structure. The reaction fronts seem thinner with ethanol than with heptane. The dataset can be used for model validation.

1. Introduction

Spark ignition of recirculating spray flames is a topic of technological importance which contains significant fundamental challenges as it involves complicated combustion phenomena [1]. In this paper we extend the investigation of Marchione et al. [2] by examining flames of various fuels, flows with and without swirl, a laser-induced breakdown for sparking rather than disturbing electrodes, and we focus on flows with higher bulk velocities. Also, fast imaging diagnostics are deployed to probe the flame structure [3]. There are various phases associated with the successful ignition of a spray burner: (i) kernel initiation; (ii) flame growth; and (iii) overall flame stabilisation. Each of these phases involves a certain stochasticity, which leads to a wide range of different behaviours for a particular spark event [1]. This study aims to measure the timescales of these individual processes, while fast OH-PLIF is also used to examine the flame structure and the development of the kernel in the first stages of growth.

2. Experimental methods

2.1 Burner

The burner was previously used by Marchione et al. [2] and slightly modified here, with a replica installed at the University of Sydney. It consists of an outer duct for air injection, a central inner duct for fuel injection, and a combustion chamber (Fig. 1). Air is injected through two opposite slots located at the top of a 35 cm long circular duct of 37 mm inner diameter. The air flow rate is set through rotameters, calibrated by a mass flow controller (Bronkhorst, IN-Flow, [0–600] L/min). The fuel line is a 6 mm inner and 10 mm outer diameter pipe centred in the outer duct. Two fuels are used successively for this study: ethanol and n-heptane. Due to the quick evaporation of the liquid fuel, it is possible to stabilize spray flames at a laboratory-scale burner without preheating air. The fuel is pressurized with nitrogen in a feeding tank and then atomized through a pressure swirl atomizer (Lechler, axial flow hollow cone nozzle). The nozzle exit diameter is 0.15 mm, the spray cone angle is 60 degrees. The fuel flow rate is set by a mass flow controller (Bronkhorst, LIQUI-flow, L30, [0–2] g/s). The nozzle is centred inside a bluff body of diameter d_{BB} = 25 mm, with a 4 mm

hole in the centre. The burner is oriented vertically downwards in order to collect safely unburnt fuel during the ignition experiments. In order to study swirling flames, a swirler (6 blades oriented at 60 degrees with respect to the flow axis) is inserted between the inner and outer ducts. The direction of the air swirl is clockwise when looking at the nozzle from the combustor. The combustion chamber has a square cross-section of side 95 mm (3.8 d_{BB}) and is 150 mm in length (6 d_{BB}). It is made of synthetic quartz designed for optical diagnostics (optically flat sides, deep UV transmission and fluorescence free grade). The outlet is open to the atmosphere.

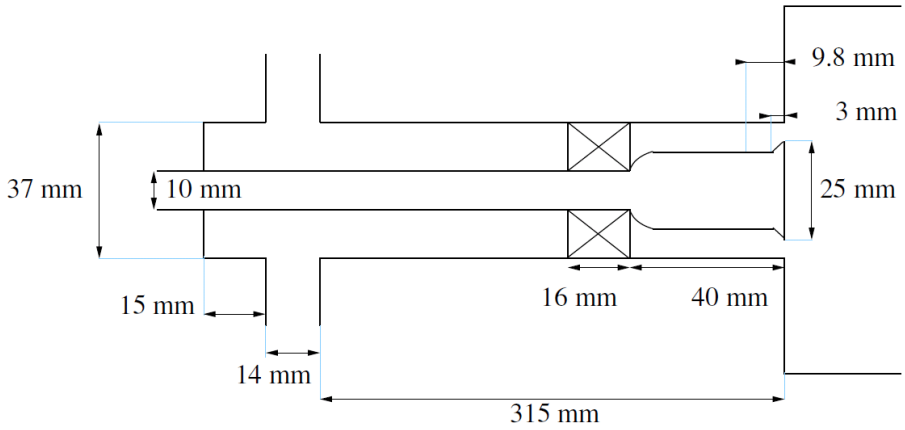

Figure 1: Sketch of the burner. The burner is oriented vertically downwards.

2.2 Spark generation

In the studies previously performed at Cambridge University, ignition was achieved by electrical sparks [1,2,4]. In this study, the spark is created by focusing the beam from an 8 ns Q-switched Nd-YAG laser (Continuum Surelite operating at 1064 nm) through a biconvex quartz lens with a 75 mm focal length and a 50 mm diameter [5]. The laser operates in the single pulse mode. The energy of the spark can be adjusted by changing the Q-switch delay. In order to get a spark for each laser spot, the energy before the focusing lens must be above a threshold that depends on the properties of the laser and the presence of particles in the environment. In case of a turbulent droplet-air mixture, the instantaneous properties of the mixture at the location of the spark can be strongly different from the mean properties. In the framework of this study, the energy is set to 140 mJ/pulse, to ensure the generation of a spark after each laser shot, for all studied flow conditions and for all locations of the spark in the combustor. The energy deposited by the spark results in plasma formation that generates radicals and ionized species which can then trigger chemical reactions and further heat release, in the case of flammable mixture.

The reference location of the spark is determined in a non-flowing air environment. Due to the presence of fuel droplets, the location of the spark may vary a bit around its nominal location. Chemiluminescence and PLIF images show that the spark may lie a few millimetres away from its location in clean air. The burner is fixed on a frame with 3-directional traverse. The location of the spark can then be changed inside the combustion chamber. Many failed and successful ignition events have been recorded by the high-speed camera. Two spark locations were investigated: “position A” is on-axis, 10 mm downstream of the bluff-body (x = 0 mm, z = 10 mm) while “position B” is 10 mm off-axis and at the same downstream station (x = 10 mm, z = 10 mm).

2.3 Flow conditions

Considering a given fuel (ethanol “E” or n-heptane “H”), two flow conditions are investigated for the non-swirling flames and three flow conditions for the swirling flames. In

the non-swirling configuration, the flow conditions are chosen depending on the spark location. Only a very small change of the air flow rate is needed to switch from a condition that enables the stabilization of a flame at every spark (condition "S") to a condition that never enables the stabilization of a flame (condition "F"). Table 1 summarizes the non-swirling flow conditions.

Table 1: Flow conditions for non-swirling flames ("BB").

Name	Fuel	$\dot{m}_{fuel}$ (g/s)	$\dot{m}_{air}$ (kg/min)	U_b (m/s)	Φ
BBE1-S	Ethanol	0.17	0.90	21.9	0.10
BBE2-F			0.97	23.5	0.09
BBH1-S	Heptane	0.12	0.74	17.9	0.15
BBH2-F			0.80	19.3	0.14
BBH3-S			1.26	30.6	0.09
BBH4-F			1.29	31.4	0.08

In the swirling configuration, the flow conditions are chosen depending on the blow-off value. Those flow conditions are independent of the spark location. Condition 1 corresponds to an air flow rate equal to 77% of the air flow rate at the blow-off condition: it is a stable flame. Condition 2 corresponds to an air flow rate equal to 89% of the air flow rate at the blow-off condition. Condition 3 corresponds to an air flow rate equal to 100% of the air flow rate at the blow-off condition: it is never possible to stabilize a flame. Table 2 summarizes the swirling flow conditions.

Table 2: Flow conditions for swirling flames ("SW").

Name	Fuel	$\dot{m}_{fuel}$ (g/s)	$\dot{m}_{air}$ (kg/min)	U_b (m/s)	U_b / U_{BO}	Φ
SWE1	Ethanol	0.17	0.65	15.8	0.77	0.14
SWE2			0.75	18.3	0.89	0.12
SWE3			0.84	20.5	1.00	0.11
SWH1	Heptane	0.12	0.59	14.3	0.77	0.18
SWH2			0.68	16.0	0.89	0.16
SWH3			0.77	18.5	1.00	0.14

2.4 Ignition probability

In the framework of this study, successful ignition is defined as a laser spark resulting in a flame kernel formation and growth, followed by flame propagation and leading to the stabilization of a flame in the whole combustor. Individual spark events do not always result in full flame establishment. Ignition is thus a probabilistic phenomenon. The random characteristic of ignition is due to different phenomena: inhomogeneous concentration of the fuel droplets and then equivalence ratio, velocity and strain rate... This is consistent with similar observations previously made for ignition of gaseous fuel in turbulent non-premixed flows [2,4,6,7] and two-phase turbulent flows [1,2]. To define the ignition probability P_{ign}, a series of trials is performed. The probability of ignition is computed as the number of successful events divided by the number of trials. For this study, the ignition probability is measured by applying 30 single sparks at each location. This involves an uncertainty of 9% at 50% ignition probability. Moving the location of the spark, it is possible to get a map of ignition for the whole combustor. Such detailed data are available only for the swirling n-heptane flames and are reported in Ref. [8]; for the other flames, P_{ign} was measured only at the points used for visualizing the kernel evolution.

2.5 High-speed imaging

Ignition events have been monitored by fast OH*-chemiluminescence and fast OH-PLIF to study the kernels growth after the end of the laser spark. Since chemiluminescence is a line-of-sight integration technique, the interpretation of data can sometimes be ambiguous. That is why the behaviour of the kernels is also examined on the burner axis by PLIF.

The system used is described with more detail in Ref. [3,8]. The detection system is similar for both chemiluminescence and PLIF records. It consists of a LaVision High-Speed Star 6 CMOS camera (HSS6, 1024x1024 pixels) fitted with a two-stage intensifier (High-Speed IRO, LaVision, 12 bits). Two UV aplanatic meniscus lenses back to back are used instead of a camera objective (clear aperture: 60.0 mm, focal length: 192.0 mm). The repetition rate of the camera is 5 kHz. The resolution of the images is 0.08 mm/px (image width: 45 mm). The highest sensitivity of the imaging system is in the UV range. To collect either OH*-chemiluminescence signal or OH-PLIF signal, the intensifier properties (gate width and delay) and the filters are chosen depending on the fuel used. The conditions of acquisition are summarized in Table 3.

To avoid intense light into the intensifier, the first OH*-chemiluminescence image is recorded 40 μs after the spark. To process the chemiluminescence images, a threshold is first defined. The value of the threshold is arbitrarily chosen from the histogram of grey levels. A binary mask is then computed: all pixels under the threshold are put to zero, all pixels equal to or above the threshold are put to one. This mask is filtered by a 3x3 px median filter. The multiplication pixel by pixel of the images and the associated masks allows noise removal without affecting the shape of the flame nor the intensity counts.

To avoid intense light into the intensifier, the beginning of OH-PLIF images is 25 μs (except for the ethanol flames where the delay varies between 5 and 40 μs). To collect the OH-PLIF signal, the OH molecule is first excited at 283 nm. A Nd-YAG laser is used to pump a SIRAH Allegro high speed dye laser. The dye is Rhodamine 6G dissolved in ethanol. The fundamental beam at 566 nm is then frequency doubled using a BBO crystal. To maximize the signal to noise ratio, the OH-PLIF is conducted in the non-linear regime. Both the flame luminosity and the laser wavelength are filtered. Images of acetone vapour were recorded before and after every set of data to get the laser beam profile. OH-PLIF images are next divided by the mean image of acetone PLIF to take in account the laser profile.

Table 3: Acquisition parameters.

	Flame type	Non-swirling (BBE, BBH)	Swirling	
			Ethanol (SWE)	Heptane (SWH)
OH* Chemi.	Gate width	3 500 ns		3 500 ns
	Gate delay	50 000 ns		50 000 ns
	Filters	UG11		UG11
OH-PLIF	Gate width	200 ns		200 ns
	Gate delay	2 100 ns		2 100 ns
	Filters	UG11, WG295, WG305		WG295, WG305

3 Results and discussion

3.1 Ignition probability

In the non-swirling burner, it is not possible to ignite a flame very close to the bluff-body ($z<4$ mm, i.e. $z<0.16\ d_{BB}$). At a given distance z from the bluff-body, the probability of ignition was found to change from 0 on the air-side to 1 in the jet over a very short distance (typically the spacing is less than the mesh grid, i.e. less than 5 mm). Thus only two

conditions with ignition probabilities of respectively zero and 100% were chosen at each spark location for the non-swirling flames, as shown in Table 4 for both ethanol and n-heptane fuels.

Table 4: Probability of ignition of the non-swirling flames for the two spark locations.

	Ethanol		Heptane	
A	BBE1A-S	P_{ign} = 100%	BBH3A-S	P_{ign} = 100%
	BBE2A-F	P_{ign} = 0%	BBH4A-F	P_{ign} = 0%
B	/		BBH1B-S	P_{ign} = 100%
			BBH2B-F	P_{ign} = 0%

In the swirling burner, it is possible to ignite a flame at various locations in the combustion chamber with different probabilities. A map of ignition probability was generated for each heptane swirling flame [8]. This map demonstrated that, for the lowest air flow rate, the proportion of successful events can reach 100% at some locations (i.e. all kernels turn into a stable flame). An increase of the air flow rate generates an increase of failed events and a decrease of successful events. The number of kernels dying very quickly after the end of the spark increases too. The probability of ignition of a stable flame P_{ign} is compared with the probability of getting a visible kernel P_{ker} (without considering its evolution i.e. extinction or growth). Note that P_{ign} is easily established by eye, while P_{ker} may be ambiguous as kernels missed by the operator may have been generated by the spark. That's why further investigation was performed by fast diagnostics to obtain more accurate statistics. From these experiments, it is evident that (i) as the air velocity increases and the blow-off condition is approached, P_{ign} decreases and reaches zero at the blow-off condition. These set of data also show that (ii) P_{ker} is equal to P_{ign} for the low velocity condition; (iii) P_{ker} is grater than P_{ign} for the high velocity conditions: kernels are generated even for the blow-off condition, but these fail to grow or, even if they do, full-flame stable ignition is not achieved. The probability of ignition for the swirling flames for the two spark locations are shown in Table 5.

Table 5: Probability of ignition of the swirling flames for the two spark locations.

	Ethanol		Heptane	
A	SWE1A	P_{ign} = 86%	SWH1A	P_{ign} = 98%
	SWE2A	P_{ign} = 70%	SWH2A	P_{ign} = 82%
	SWE3A	P_{ign} = 0%	SWH3A	P_{ign} = 0%
B	SWE1B	P_{ign} = 32%	SWH1B	P_{ign} = 28%
	SWE2B	P_{ign} = 28%	SWH2B	P_{ign} = 8%
	SWE3B	P_{ign} = 0%	SWH3B	P_{ign} = 0%

3.2 Visualization of ignition events

Many failed and successful ignition events have been recorded by the high-speed camera. From chemiluminescence records, it seems that the behaviour of the kernel after the end of the spark is generally the same for a given burner configuration no matter what the fuel is, despite the fact that ethanol vaporizes quicker than n-heptane. Instantaneous individual images are not representative of all the information visible in the high-speed movies, but they show samples of the behaviours of the kernel and the flame. The typical evolution of the kernel is described below.

Chemiluminescence images show line-of-sight information. Due to soot emission and long camera exposure, the structure of the flame front is not clearly visible on the OH*-chemiluminescence images. Thus, ignition was also investigated through OH-PLIF records. Information is recorded in the plane crossing the burner axis.

Non-swirling flames

Figure 2 shows typical snapshots of OH*-chemiluminescence images for a successful spark event in a non-swirling flame. After the end of the spark, the kernel starts growing and the intensity decreases. The kernel then moves upstream and takes a few tens of milliseconds to reach the bluff body. The kernel continues to grow and eventually, the whole combustor is ignited. Records of the n-heptane flame show a very small kernel that sometimes disappears almost completely. The difference of kernel size between ethanol and n-heptane flames is possibly due to the vaporisation properties of the fuel. It takes a bit longer for the n-heptane kernel to reach the bluff-body (relative to ethanol kernels). However, the evolution of the kernel into a stable flame is quicker with n-heptane. The maximum intensity is found on the edges of the flame and along the spray cone.

A kernel leading to misfire is usually a bit smaller than a kernel leading to successful ignition. After the end of the spark, the emission intensity decreases. The kernel does not grow and sometimes its size even decreases on the first images. Some records of n-heptane show the initial kernels splitting into separate smaller kernels. Considering flow condition BBH4-F (highest air velocity), the kernel is less likely to split and the intensity decreases more slowly than in the other flow conditions.

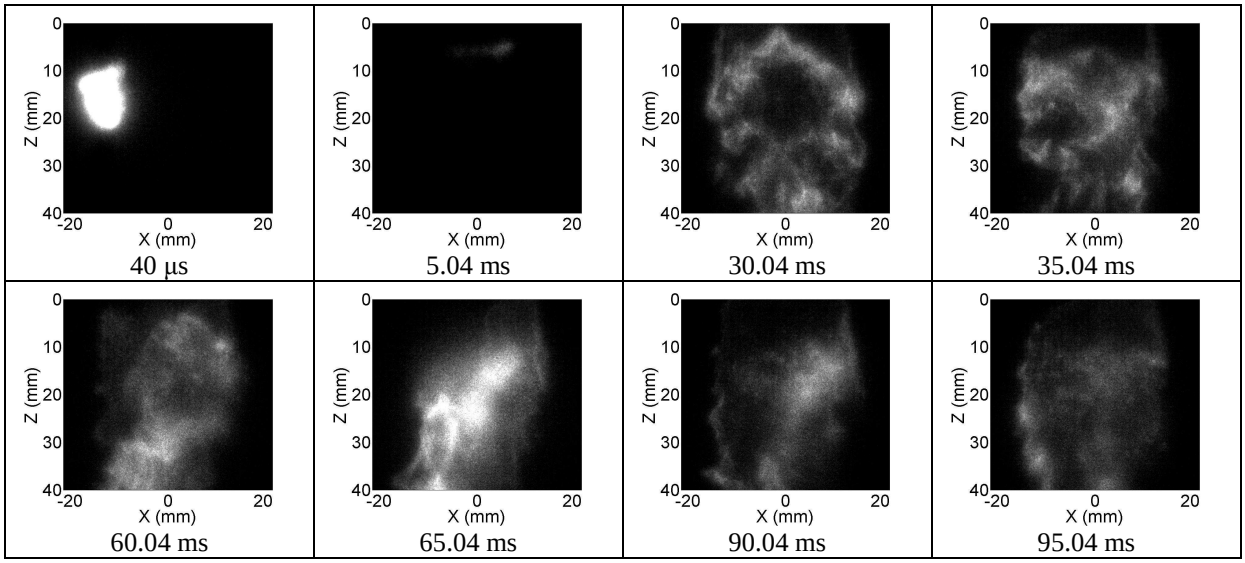

Figure 2: Typical snapshots of OH*-chemiluminescence of non-swirling n-heptane flames (BBH1B-S).

Figure 3 and 4 show typical snapshots of OH-PLIF images for a successful spark event in the non-swirling configuration. The behaviour of the kernel is different depending of the location of the spark initially. For a spark in position A, the kernel usually stays in the laser plane. Sometimes the kernel stagnates at the location of the spark but then moves quickly towards the bluff-body. For a spark in position B, images show that the kernel grows in all directions and often moves out of plane. The initial kernel splits into smaller parts most of the time. One of them anchors on the bluff-body. Images also show a different structure depending on the fuel. Ethanol flames exhibit a flame front that is continuous, thin and very distorted. Once the flame is stabilised, the OH signal is mainly located at the edges of the bluff-body (Fig. 3). Heptane flames present a flame front slightly thicker and patchier. The flame front is distorted too. But the main difference is the presence of OH in the area in the wake of the bluff-body that appears and disappears (Fig. 4). A double flame structure is sometimes visible and the flame front seems to follow the spray cone.

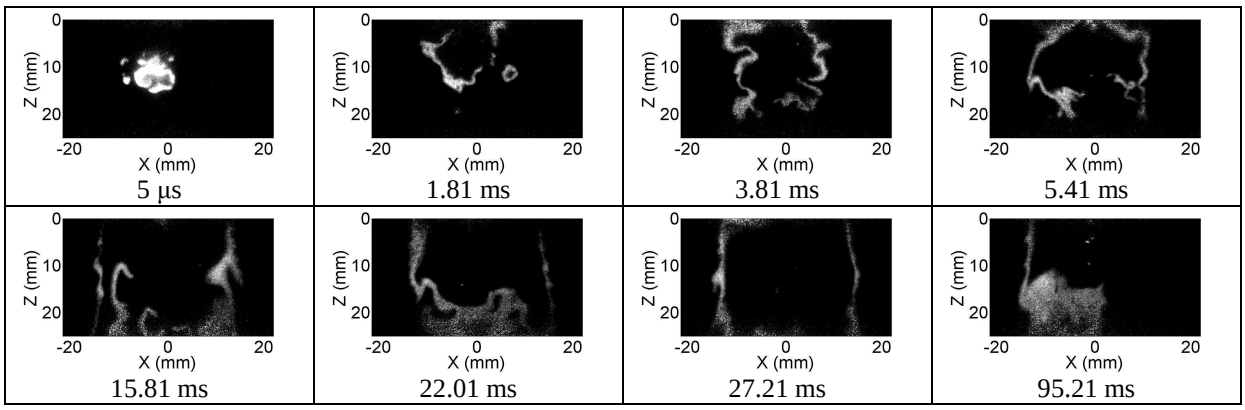

Figure 3: Typical snapshots of OH-PLIF of ethanol non-swirling flames (BBE1A-S).

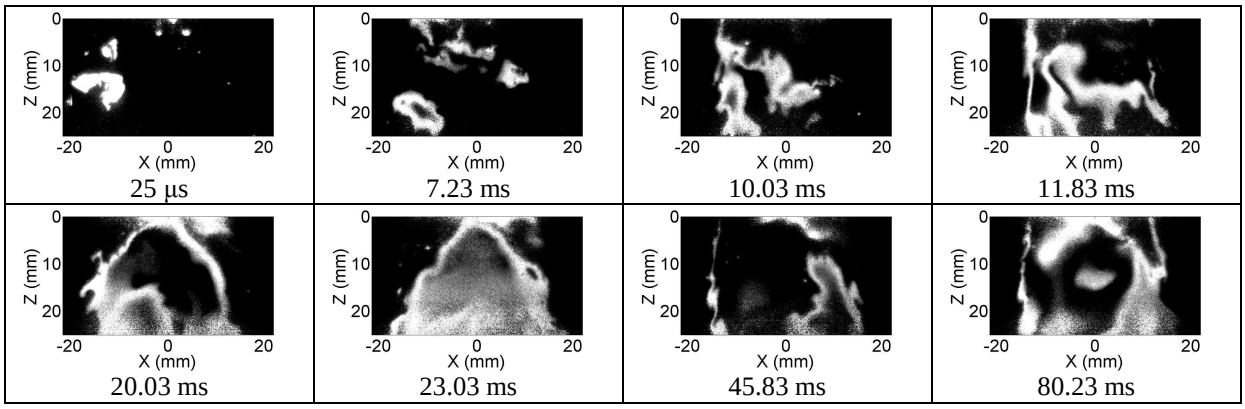

Figure 4: Typical snapshots of OH-PLIF of n-heptane non-swirling flames (BBH1B-S).

Swirling flames

The three flow conditions were investigated by OH*-chemiluminescence first. Figure 5 shows typical snapshots of OH*-chemiluminescence for a failed spark event in the swirling burner.

Considering flow condition 1 (with either fuel, i.e. SWE1 or SWH1) that is far from blow-off, it seems that the behaviour of the kernel during the first stages of growth, and next during propagation, depends more on the ignition location relative to the recirculation zone, rather than on the flow condition. When the spark is located in position A (on the axis), the kernel moves quickly upstream and seems to be a bit larger. It takes only a couple of milliseconds for the kernel to reach the bluff-body. As observed for the non-swirling flames, the intensity of the kernel decreases a bit after the end of the spark. It is even possible to have a few dark frames considering n-heptane kernels, especially if the spark is located in position B. Comparing positions A and B, by the time a spark initiated at the location A has reached the bluff-body, a spark initiated at the location B is almost not visible any more. A few frames later, a kernel re-appears close to the bluff-body. Some ten milliseconds after the laser spark, the kernel is anchored on the bluff-body and starts growing. On the one hand, the growth of the kernel is more slowly for n-heptane flames. But on the other hand, the development of the kernel into a stable flame is quicker. In case of misfire, the kernel does not move after the end of the spark. Usually the kernel is smaller than kernels leading to successful ignition. If the spark was located in position A, the kernel size will evolve rapidly. On the other hand, if the spark was located in position B, the size of the kernel is not likely to evolve before reaching the bluff-body. The intensity is very low and it decreases with time.

Considering flow condition 2, the behaviour of the kernel is very similar to flow condition 1 when the spark is located in position A, but the development of the flame is longer when the spark is located in position B. The following phenomena are visible for most of the records: (i) once the kernel has reached the bluff-body, its size grows considerably; (ii) motions of some "arms" to the left and to the right are visible. Some rotating motions can happen too; (iii) from time to time, some burning zones are detached from the main flame and extinguished. Some zones of high intensity can also appear in the reacting zone.

Considering failed events (Fig. 5), is not possible to distinguish between successful or failed ignition looking only at the very first frames of flow condition 2. However the kernel is very likely to disappear either in a few or some tens of frames.

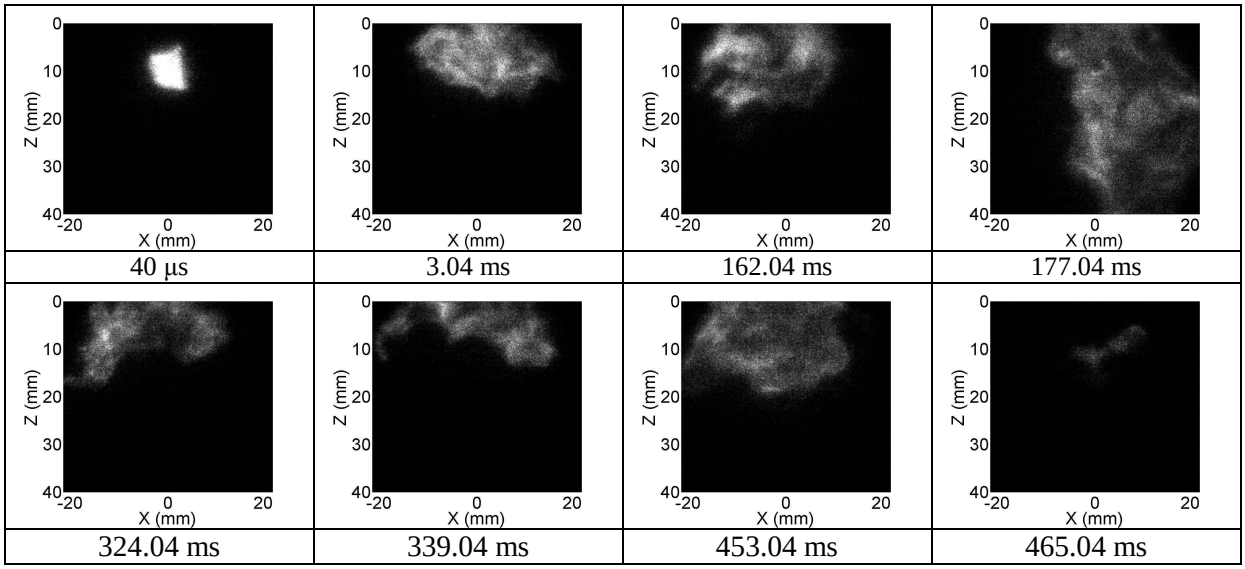

Figure 5: Typical snapshots of OH*-chemiluminescence of swirling flames (failed, SWE2A).

The evolution of the kernels in flow condition 3 (blow-off condition) is much more stochastic. Images extracted from high-speed movies of swirling flames (either n-heptane or ethanol) show that failure occurs in a (i) "short failure mode", where the kernel sometimes extinguishes before reaching the bluff-body, (ii) a failure at intermediate times and (iii) a failure at very long times after the spark. The timescales associated with the above transients and derived from OH*-chemiluminescence records are analysed in the following section.

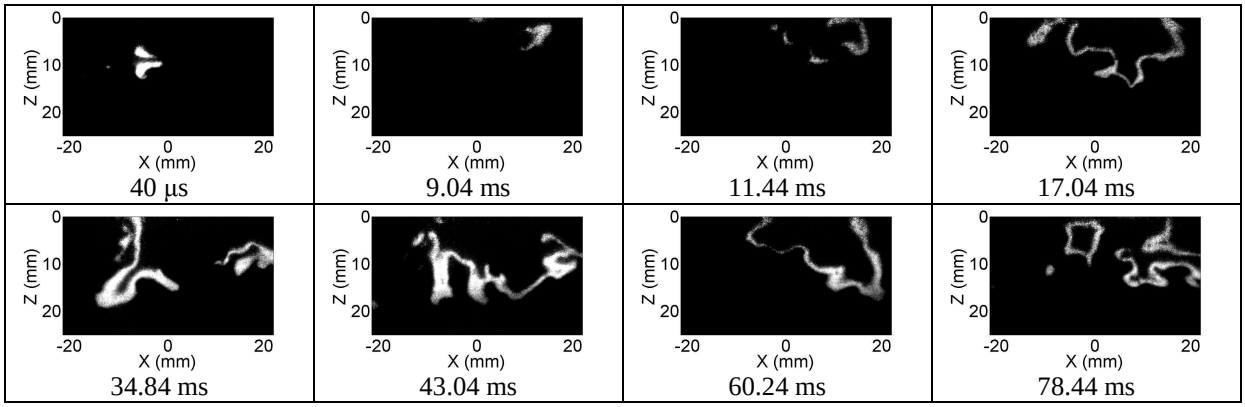

Figure 6: Typical snapshots of OH-PLIF of ethanol swirling flames (SWE2B).

The OH-PLIF images of the swirling flames show that the kernel grows in all directions from the spark location, while the reaction zone (likely to be the region of strong OH signal) is thin, very distorted, and eventually becomes anchored at the edge of the bluff-body. Very strong temporal fluctuations are evident (Fig. 6 and 7). A reaction zone going across the burner is evident, but it seems broken occasionally, which may point to the presence of localized extinctions or fuel starvation. The broken OH sheet is consistent with the fact that this flame condition is close to blow off and is consistent with imaging in gaseous non-premixed flames close to extinction [3].

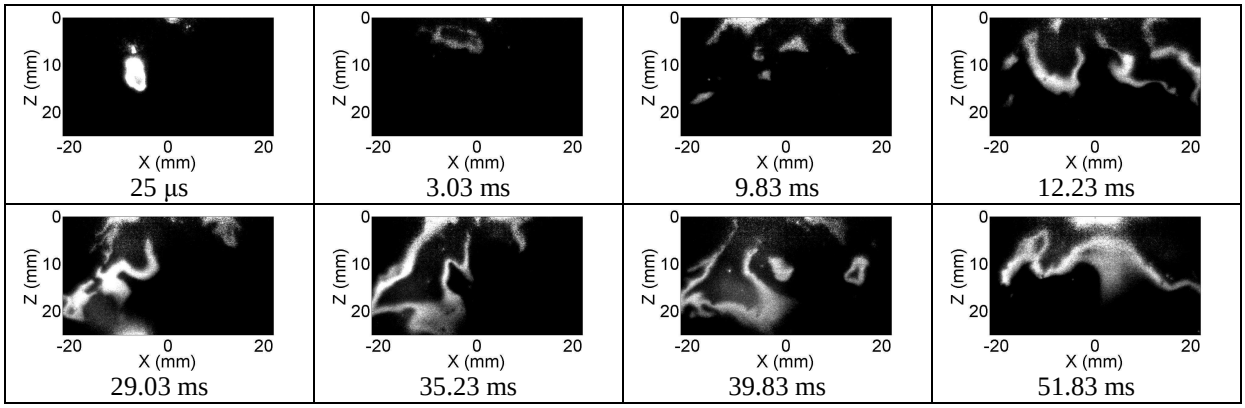

Figure 7: Typical snapshots of OH-PLIF of heptane swirling flames (SWH1B).

Finally, we note that playback and some limited quantitative analysis of the OH* movies of the stable flames reveals a low-frequency wobbling motion of the flame, where long "arms" such as the right flame branch in Fig. 7 (29.03ms) or the left branch in Fig. 7 (51.83ms) seems to periodically swing left to right. Such a motion may be associated with a precessing vortex core. Velocity measurements can help the interpretation the flame propagation behaviour. It would be of great help to have gaseous global equivalence ratio measurements as well as droplets size and velocity data to better understand the ignition kernel behaviour and the flame structure.

3.3 Time scales

Three time scales were defined from the OH*-chemiluminescence records: kernel initiation, full flame ignition and extinction. To be characteristic of the phenomenon they describe, the time scales have to be objective. The methods used here are applicable to all studied conditions. They were initially developed for the swirling heptane flame [8] but are applicable to all the studied conditions. The time scales are defined from the evolution of the intensity in the image versus time as described below. Figure 8-a shows a typical example of the evolution of the area-integrated OH*-chemiluminescence of a successful event versus time, I(t).

Initiation time scale

"Initiation" is used to describe the development of the spark into a kernel that is growing in time. Initiation can only be achieved once the flame is attached to the bluff-body. Two methods are used and compared. The first method compares the evolution of the surface emitting some OH* signal S(t) and the mean area defined for a stable flame in the same flow condition, $\bar{S}$. The time scale of initiation, τ_{in1}, is defined as the time when the curve S(t) reaches the value $0.75\bar{S}$ (Fig.8-b). In the alternative definition, the time scale of initiation, τ_{in2}, is defined as the time when the curve of intensity counts, I(t), reaches the first local

maximum (Fig.8-c). The values of τ_{in1} are a bit lower than that of τ_{in2}. Initiation is generally achieved within tens of milliseconds, most of the time in less than 10 ms (Tables 6 and 7). The order of magnitude is very similar for both fuels and both burners.

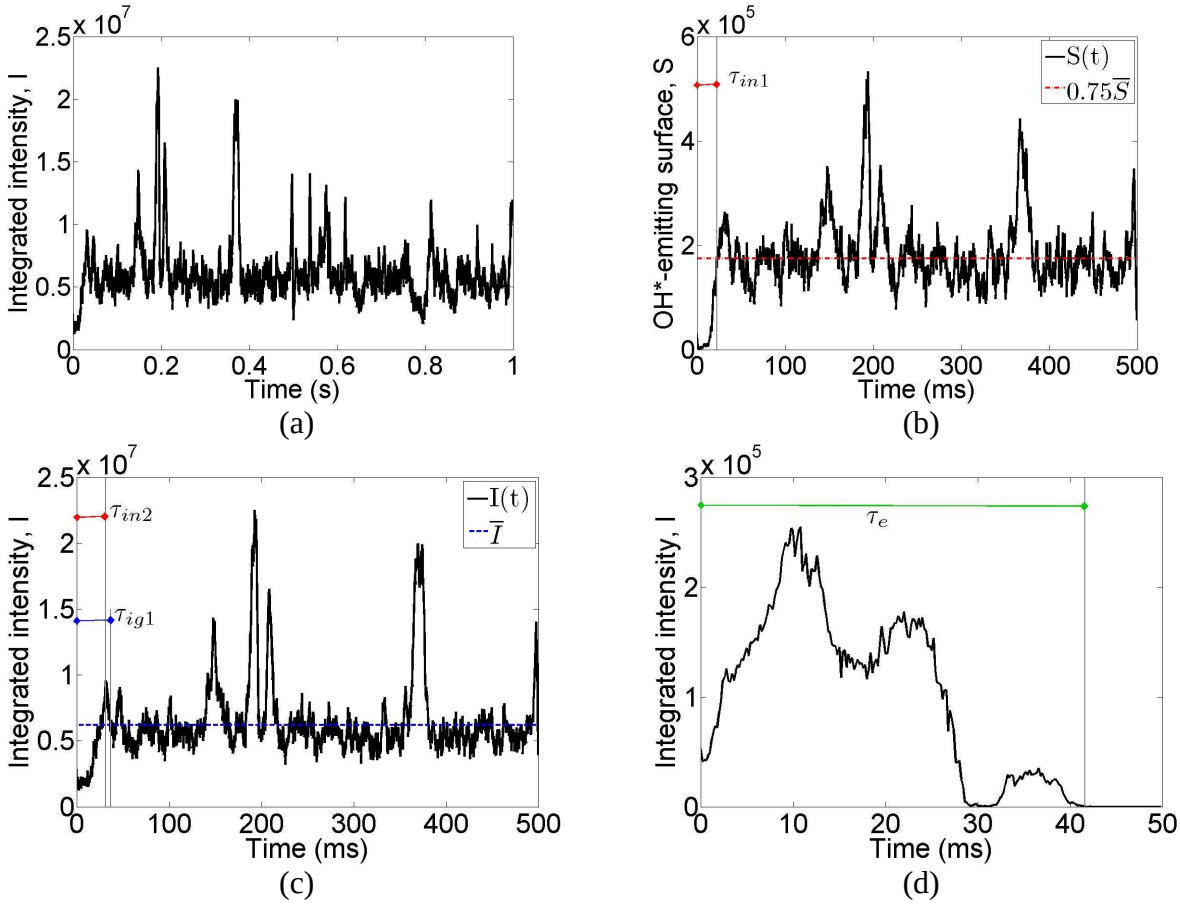

Figure 8: (a) Typical area-integrated OH*-chemiluminescence of a successful event; (b) Definition of the initiation time scales τ_{in1}; (c) Definition of the initiation time scales τ_{in2} and ignition time scales τ_{ig1}; (d) Definition of the extinction time scale, τ_e.

Table 6: Range of time scale of kernel initiation of the non-swirling flames.

		τ_{in1}	τ_{in2}
BBE1-S	A	[2; 27] ms	[3; 14] ms
BBE3-S		[10; 24] ms	[4; 27] ms
BBH1-S	B	[5; 16] ms	[4; 23] ms

Table 7: Range of time scale of kernel initiation of the swirling flames.

			τ_{in1}	τ_{in2}
Success	SWE	A	[2; 39] ms	[19; 41] ms
	SWH		[4; 6] ms	[8; 16] ms
	SWE	B	[6; 7] ms	[7; 11] ms
	SWH		[6; 18] ms	[7; 32] ms
Failed	SWE	A	[2; 8] ms	[14; 29] ms
	SWH		[3; 7] ms	12 ms
	SWE	B	[7; 24] ms	[3; 27] ms
	SWH		[4; 24] ms	[5; 16] ms

Full flame ignition time scale

We consider that "full flame ignition" is achieved once the global behaviour of the flame is constant in time. Here again, we compare two methods. The first definition, τ_{ig1}, corresponds to the time when the curve I(t) reaches its average value $\overline{I}$ (Fig.8-c). The second definition comes from individual image viewing. Using the images of the movies, the time scale of full flame ignition, τ_{ig2}, is defined as the time needed to get a fully developed symmetrical flame anchored on the bluff-body. The values of τ_{ig1} and τ_{ig2} are in good agreement. In case of non-swirling flame, this definition is applicable to successful events only. On the other hand, in swirling flames, flame stabilisation is possible for some failed events. Kernels corresponding to successful events are stabilized more quickly than kernels corresponding to failed events. The range of values is summarized for all conditions in Tables 8 and 9. Considering a spark located in position A, the nature of the fuel does not influence too much the time scale. However, we can notice a slight difference when the spark in located in position B for the swirling flames: in case of a successful event, full flame ignition is achieved more quickly if the fuel is ethanol; while in case of a failed event, full flame ignition is not achieved. However, the stabilisation of the flame on the bluff-body is achieved more quickly if the fuel is heptane.

Table 8: Range of time scale of full flame ignition of the non-swirling flames.

		τ_{ig1}	τ_{ig2}
BBE1-S	A	[6:17] ms	[4:18] ms
BBH3-S		[3:21] ms	[4:19] ms
BBH1-S	B	[2:8] ms	[6:11] ms

Table 9: Range of time scale of full flame ignition of the swirling flames.

			τ_{ig1}	τ_{ig2}
Success	SWE	A	[11:15] ms	[4:6] ms
	SWH		[1:5] ms	6 ms
	SWE	B	[4:6] ms	[7:15] ms
	SWH		[5:27] ms	[5:24] ms

Extinction time scale

The time scale of extinction is the simplest to determine. However great care is required as the images can be totally dark at some point whereas the flame is not extinguished yet. In fact, some curves present a decrease to zero and then an increase of the intensity counts, but this lasts less than a few milliseconds (Fig.8-d). Thus τ_e is defined as the time for which the curve of intensity goes down to zero and stays equal to that value for at least 15 ms. The movies show three time scales differing by orders of magnitude: (i) short failure mode: from a few microseconds to a few milliseconds; (ii) intermediate mode: a few tens of milliseconds; (iii) long failure mode: hundreds of milliseconds.

In case of non-swirling flames, the short failure mode is the only mode reported. The range of values is summarized for all conditions in Tables 10 and 11.

Table 10: Range of time scale of flame extinction of the non-swirling flames.

		Short failure
BBE2-F	A	[2:6] ms
BBH4-F		[1:10] ms
BBH2-F	B	[1:6] ms

Table 11: Range of time scale of flame extinction of the swirling flames.

			Short failure	Intermediate failure	Long failure
Failed	SWE	A	[5:6] ms	[34:58] ms	[464:835] ms
	SWH		2 ms	[9:42] ms	[341:492] ms
	SWE	B	[2:5] ms	[10:23] ms	[468:597] ms
	SWH		1 ms	6 ms	[362:698] ms

4 Conclusions

An experimental study of laser ignition on lab-scale non-swirling and swirling spray flames has been conducted. Ethanol and n-heptane were used as fuel and the behaviour of the flames was compared. Fast OH*-chemiluminescence movies allowed a classification of successful and failed events. Time-scales of initiation, full flame ignition and extinction were also extracted from the movies. Concerning the non-swirling flames, the ignition behaviour is relatively simple: the small kernel generated by the spark either stabilises on the bluff-body or dies within less than 10 ms. Considering the ignition behaviour of swirling flames, it was found that spark kernels either die very quickly after the end of the spark, or survive during some time and move inside the combustor, or develop into a stable flame. For both fuels, three extinction modes were identified: short, intermediate and long failure modes.

Fast OH-PLIF records at 5 kHz identified the motion of thin flame sheets. Ethanol flames exhibit a front flame that is virtually continuous, thin and distorted and attached to the bluff-body edge. Heptane flames present a flame front that is thicker and a double flame structure, with a front approximately following the spray injection angle and another attached to the bluff body-edge. The swirling flames show a low-frequency wobbling motion that is attributed to the possible presence of a precessing vortex core.

The data can assist the validation of numerical simulations for spray ignition and stable combustion problems.

References

[1] E. Mastorakos, *Ignition of turbulent non-premixed flames*, Prog. Energy Combust. Sci., 35:57-97 (2009)

[2] T. Marchione and S.F. Ahmed and E. Mastorakos, *Ignition of turbulent swirling n-heptane spray flames using single and multiple sparks*, Combust. & Flame, 156:166-180 (2009)

[3] M. Juddoo and A.R. Masri, *High-speed OH-PLIF imaging of extinction and re-ignition in non-premixed flames with various levels of oxygenation*, Combust. & Flame, 158:902-914 (2011)

[4] S.F. Ahmed, R. Balachandran, T. Marchione, and E. Mastorakos, *Spark ignition of turbulent non-premixed bluff-body flames*, Combust. & Flame, 151:366-385 (2007)

[5] C. Letty, A. Pastore, E. Mastorakos, R. Balachandran, and S. Couris, *Comparison of electrical and laser spark emission spectroscopy for fuel concentration measurements*, Exp. Therm. Fluid Sci., 34:338-345 (2010)

[6] S. Ahmed, E. Mastorakos, *Spark ignition of lifted turbulent jet flames*, Combust. & Flame 146:215–231 (2006)

[7] S. Ahmed, R. Balachandran, E. Mastorakos, *Measurements of ignition probability in turbulent non-premixed counter flow flames*, Proceedings of the Combustion Institute 31:1507–1513 (2007)

[8] C. Letty, E. Mastorakos, M. Juddoo, W. O'Loughlin and A.R. Masri, *Structure and timescales of igniting heptane spray swirling flames*, ICDERS 2011, Irvine, California, USA